ASTRO-H

INSTRUMENT CALIBRATION REPORT
Telescope Definition File & Optical Constant
ASTH-SXT-CALDB-MIRROR

Version 0.1

12 August 2016

ISAS/GSFC

Prepared by: Y. Maeda, R. Iizuka, T. Hayashi, T. Okajima, H. Mori

Table of Contents

CHANGE RECORD PAGE (1 of 2)

DOCUMENT TITLE: Telescope Definition File and Optical Constant.			
ISSUE	DATE	PAGES AFFECTED	DESCRIPTION
Version 0.1	June 2016	All	CALDB First Release
Version 0.2	August 2016	Section 3.1	Add affective area figure

1 Introduction

1.1 Purpose

This document describes only the elements and structure of the two Soft X-ray Telescopes (SXT) associated to the SXS and SXI on-board HITOMI that can be directly linked to their performance. It also explains how these are implemented in the ray-tracing code (task named *xrtraytrace*) and gives the instruction to create the CALDB files used by *xrtraytrace*. The CALDB file structure is define in the ASTH-SCT-04 and available from the CALDB web page at http://hitomi.gsfc.nasa.gov.

1.2 Scientific Impact

The SXT consists of two parts (primary and secondary). Each part is divided into 4 segments containing 203 reflector shells nested around the focal point. Each edge of the reflectors in a segment (top and bottom) is maintained in alignment by 7 radial bars. Each of the fan-shaped regions sectioned by neighboring alignment bars is defined as a 'sector'. Each position of these alignment bars is tuned to optimize the X-rays focus. Errors in the alignment associated to each reflector come from both radial and tangential directions. Those errors and remaining misalignments cause a scattering and blurring of the images focused by each of local parts of the aperture of the telescope. Because the blurring varies from position to position, the reflectors are divided into 224 local regions and images are evaluated in the each of these local regions.

For a given energy and incident angle, the reflectivity of the front surface depends on the interfacial roughness, the density, and the atomic scattering factors f1 and f2. These parameters do not largely vary from reflector to reflector. Thus the reflectivity is measured from a single “standard” sample.

For a backside and a pre-collimator the image-blurring and reflectivity are complex and cannot not be easily reproduced by a physical model. They are instead measured for the “standard” sample and modeled with empirical formula.

Telescope overall performance such as its effective area, vignetting function, Point Spread Function (PSF) and Encircled Energy Function (EEF) strongly depends on the local properties of front-side of the reflectors. In the ray-tracing code (*xrtraytrace*), each reflector is defined as a series of nested sub-foils, and each sub-foil is assigned an independent position, reflector direction, reflection profile, and multilayer structure. These parameters associated with each sub-foils allows a precise performance estimation of the telescope.
In this context, CALDB files contain the information derived from the measurements necessary to reproduce the performance of the SXT-S/-I.

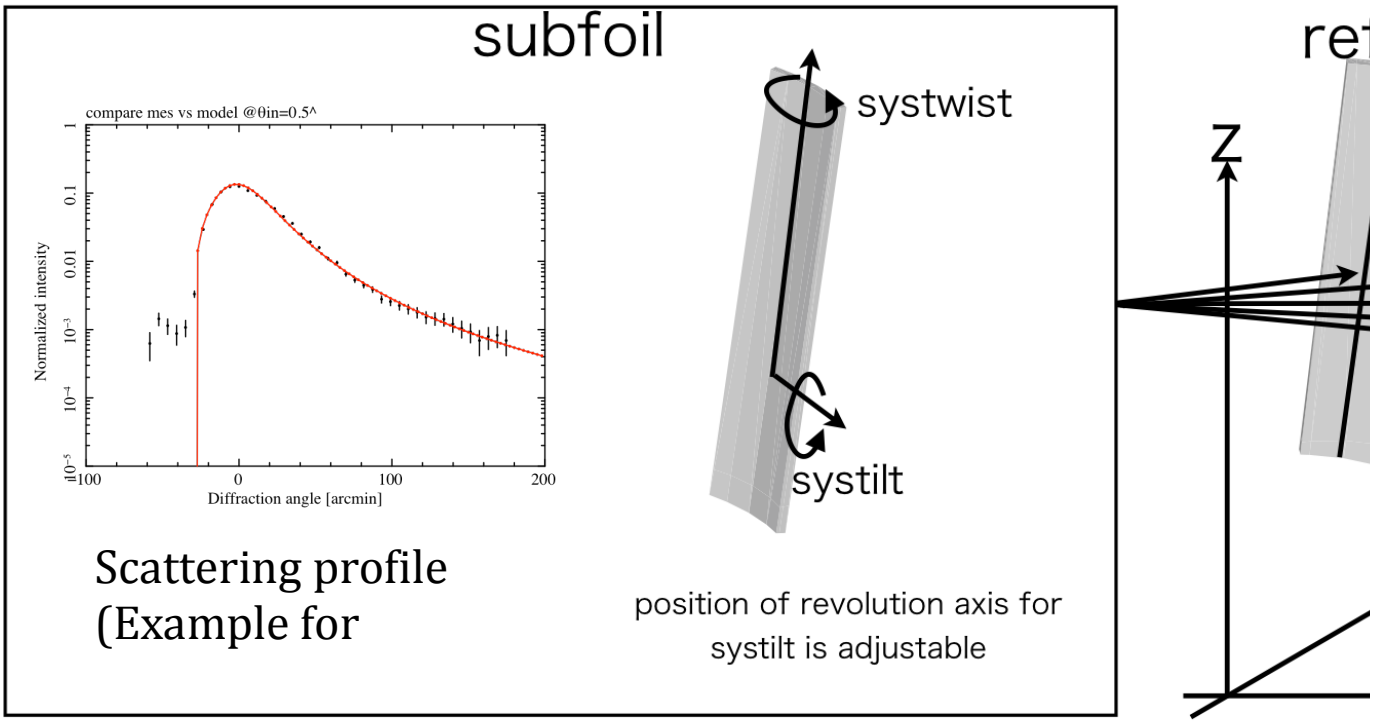

Fig. 1.1 Ray-tracing parameters, scattering profile, systilt, and systwist.
(from the HXT document.)

1.3 Contents of CALDB files

MIRROR file:

The mirror file contains the following 6 extensions.

1. **MIRROR** extension contains definitions of sub-foils and their parameters for reflectors. A sub-foil is defined as a 'sector' part of a reflector defined by alignment bars. The definition of sub-foil unit is commonly used for a primary reflector, a secondary reflector and a pre-collimator blade. The following parameters are defined for each sub-foil.
   a) Positions of edge points in cylindrical coordinate. Design values are stored.
   b) Names of reflectivity tables for the front side and back side of reflectors. A reflectivity table for a front side is calculated for each multilayer group. For the back side, it is defined to refer the common reflectivity table.
   c) Name of the reflection profile table for the front side of reflectors. Aperture is divided into regions defined with the boundaries of multilayer groups and sector boundaries (the alignment bars), and the common reflection profile is defined for primary and secondary sub-foils in each region.
   d) Misalignment in the direction of tilt and twist. In the current version, they were derived from flux-weighted mean of centroids of spot images (see 2.2). They may be tuned according to in-flight EEF (PSF) calibration.

2. **OBSTRUCT** extension contains the definitions of support structures obstructing a photon. These support structures such as alignment bars and sector covers are implemented in the code as a plane blocking photons. This plane is defined by the X-Y

coordinates of its vertexes and the plane's Z coordinate. Therefore, the plane is parallel to an X-Y plane. Design values are stored.

3. **SEGMENT** extension contains the definitions of misalignment of each segment. The displacement and orientation of each segment from the design value are defined. In the current version, design values are stored (displacement and orientation = 0). They may be tuned according to in-flight effective area, vignetting and EEF (PSF) calibration.

4. **COLLIMATOR** extension contains the definitions of sub-foils and their parameters for pre-collimator blades. The definition of sub-foil is the same as that of a reflector. For both front and back sides, the same reflectivity table and reflection profile are defined to be referred as those for back side of reflectors. They may be tuned according to in-flight effective area, vignetting and EEF (PSF) calibration.

5. **SURFACE** extension contains the definitions of mono/multilayer structure and its interfacial roughness. The design values of multilayer structures are stored. The roughness parameters are derived to fit the energy dependence of the effective area of each multilayer group according to the ground calibration data. These parameters can be tuned according to in-flight effective area calibration.

6. **AZIMUTHALSTRUCT** extension contains definitions of thermal shield geometry and materials design values are stored.

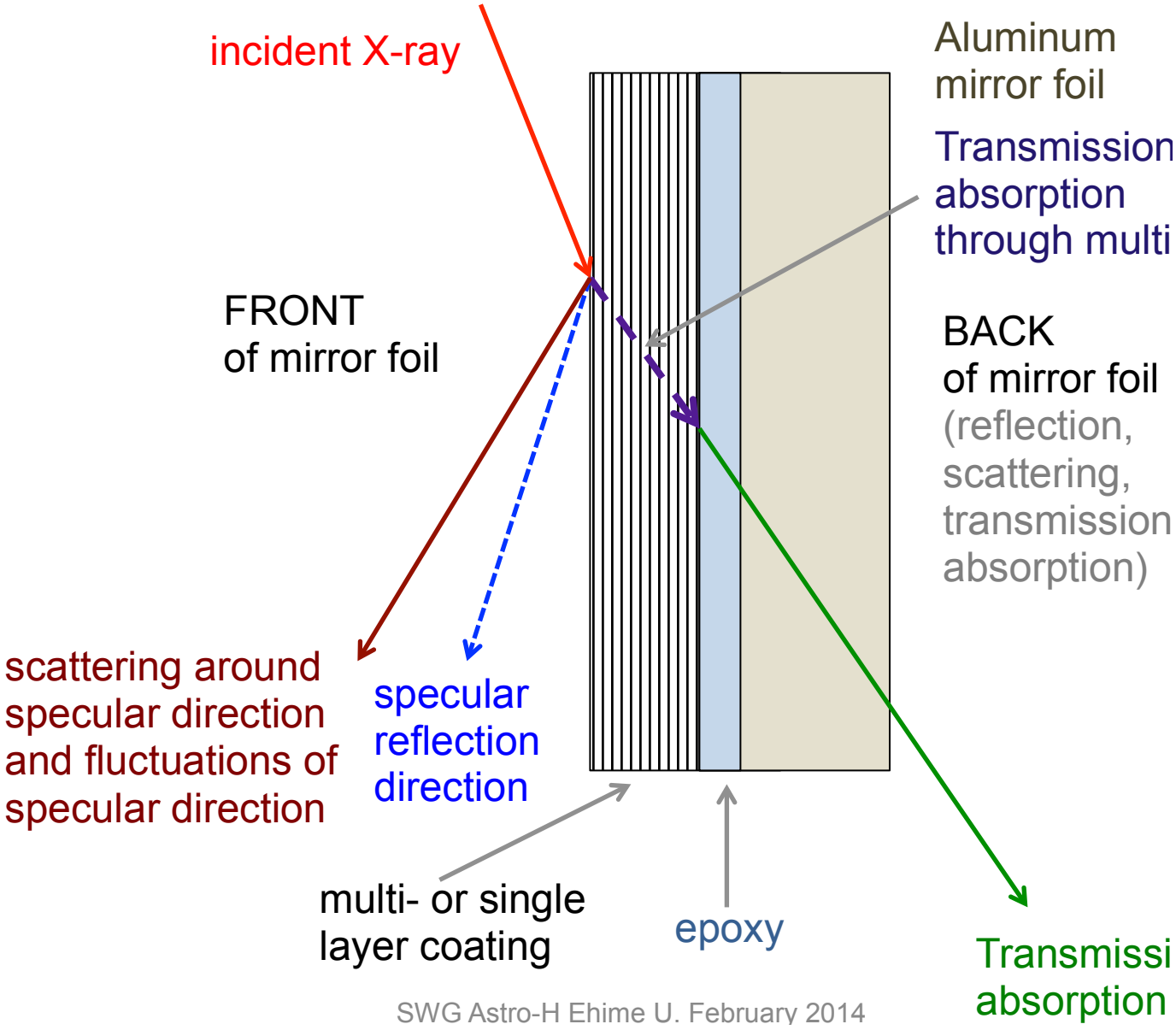

Fig. 1.2 X-ray/Mirror Interaction: Processes Considered (T. Yacoob 2014)

SCATTER file contains the reflection profiles for front side and back side of reflectors and pre-collimator blades. Front side reflection profiles were determined by on-ground measurement data (see 2.2). They may be tuned according to in-flight effective area, vignetting and EEF (PSF) calibration. For the backside of the reflector and the precollimator blades, no energy dependence is considered.

REFTRANS file contains the reflectivity and transmissivity tables for all multilayer groups calculated by *xrtreftable* with the current CALDB files, reflectivity tables for back side of reflectors and both side of pre-collimator blades, and mass absorption coefficient table for the thermal shield and the central cover.

ATOMICSCATTERING file provides various tables of atomic scattering factor (f1 and f2) from different literatures. Simulation results in this document and deriving optimum

interfacial roughness were obtained with atomic scattering factors in the extension 'HENKEMODSXT' in the current atomicScattering file. The scattering factor in 'HENKEMODSXT' come from the combination of our original measurements (KEK in SPRING-8 see below) and Henke 1993 (Atomic Data and Nuclear Data Tables Vol. 54 (no.2), 181-342) as follows.

Energy band	Tables/Edges	Sources
0.010-2.220keV	henke2013	f1,f2:henke original
2.220-2.355keV	M-V,IV	f1:KEK(0.25eV pitch), f2:henke2013
2.355-3.628keV	M-III,II,I	f1:KEK(2eV pitch), f2:henke2013
3.268-11.30keV	henke2013	f1,f2:henke original
11.30-14.00keV	L-III,II	f1,f2:SPRING-8(~0.5eV pitch)
14.00-14.90keV	L-I	f1:SPRING-8(~0.5eV pitch) f2 henke2013
14.90-30.00keV	henke2013	f1,f2:henke original

2 Release CALDB 20160310

Filename	Valid data	Release data	CALDB Vrs	Comments
ah_sxs_mirror_20140101v001.fits	20140101	20160310	001	Mirror
ah_sxs_scatter_20140101v001.fits	20140101	20160310	001	Scatter
ah_sxs_reftrans_20140101v001.fits	20140101	20160310	001	Reftrans
ah_gen_atmsca_20140101v001.fits	20140101	20160310	001	Atomic Scatter
ah_sxi_mirror_20140101v001.fits	20140101	20160310	001	Mirror
ah_sxi_scatter_20140101v001.fits	20140101	20160310	001	Scatter
ah_sxi_reftrans_20140101v001.fits	20140101	20160310	001	Reftrans

2.1 Data Description

The reflectivity of the front-side of the reflector was taken with reference samples. The reflectivity with a fine energy pitch around the gold edges was measured at the synchrotron facility: M-edges at KEK BL11B[1] and L-edges at Spring-8-BL01B1[2]. The reflection and scattering profile (hereafter scattering profile) are measured at the ISAS BeamLine (BL) facility[3].

The reflectivity and scattering profile of the backside of the reflector and the pre-collimator blade were measured at the ISAS BL, too. The over-all performance of the telescope, such as the effective area, vignetting function and image, was also measured at the ISAS BL. During the measurements, the central cover and the thermal shield were removed. The boundary covers between the quadrants are also replaced to a non-flight model. The other components, the pre-collimator and the main body (i.e., the primary and secondary reflectors) are in the flight use.

2.1.1 Reflectivity

The reflectivities of the front-side reflectors are taken at a different energy and at a different incident angle. The reflectivities around the gold M and L edges are plotted below.

[1] http://pfwww.kek.jp/kitajima/sx/bl11b_e.html

[2] http://bl01b1.spring8.or.jp/manual/BL01B1opticsmanEng041221.html

[3] Hayashi et al. J. Astron. Telesc. Instrum. Syst. 1 (4), 044004, 2015

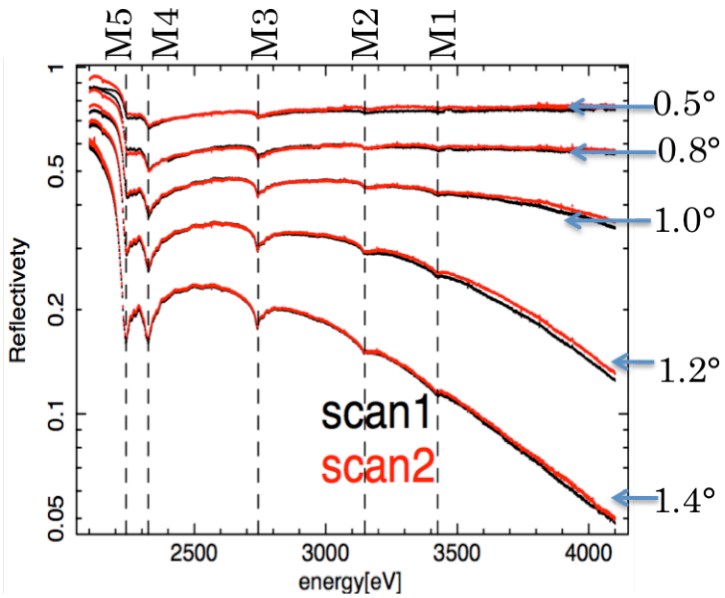

Fig. 2.1 The reflectivity measurements around the gold M-edges (Kurashima et al. 2016 SPIE Edinburgh)

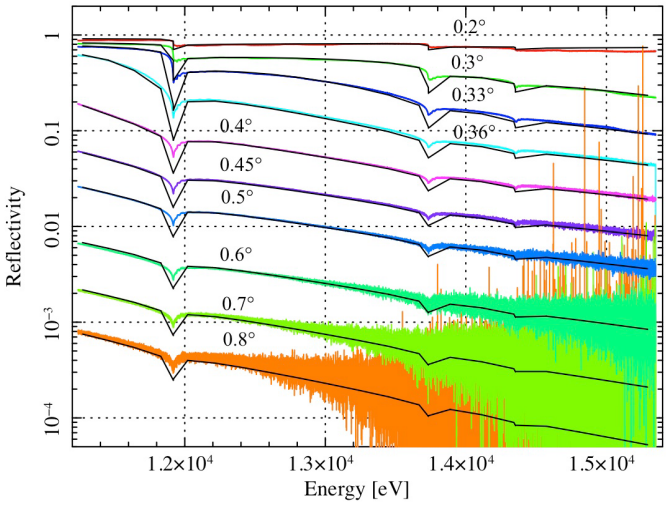

Fig. 2.2 The reflectivity measurements around the gold L-edges[4]. The colored data are our measurements whereas the black data are calculated using the HENKE table.

The reflectivities of the backside of the reflector and the pre-collimator blade are also measured at three energies. They are plotted below. The reflection below the Al-K edges are less effective because the critical angle of the aluminum material used in the backside and pre-collimator is not as large as that of the gold.

[4] Kikuchi et al. 2016, Optical Express

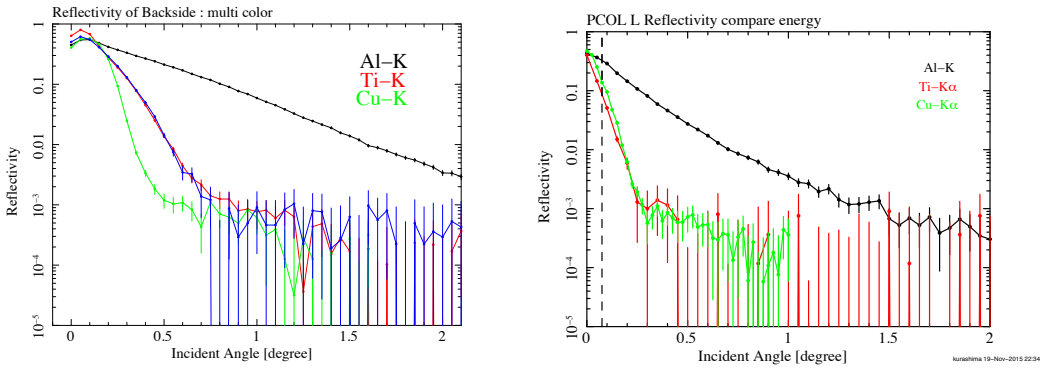

Fig. 2.3 Reflectivity of backside(left) and pre-collimator(right) at 1.49 keV (Al-K), 4.51 keV (Ti-K) and 8.04 keV (Cu-K), respectively. (Kurashima 2014 Graduation Thesis)

2.1.2 Scattering profile

The scattering profiles in large-scale are measured for the front- and back-side reflectors and the pre-collimator blade. The largely scattered component is always dim requiring a data acquisition with long exposure and with a robust integrated area. Since the reflectivity above 1.5 keV of the backside and pre-collimator is not effective, no useful data above 1.6 keV in statistics are obtained.

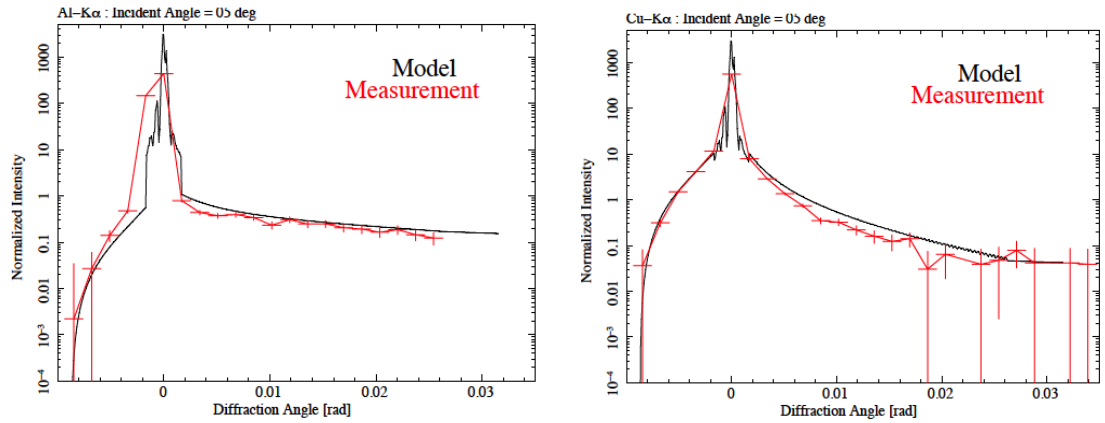

Fig. 2.4 The scattering profile (large-scale scattering/reflection profile) of the front side at 1.49 (left) and 8.04 keV (right). The typical scale of the scattering profile is 0.002 rad/ 7 arcmin. The red point corresponds to the measurements. The black line corresponds to our model.

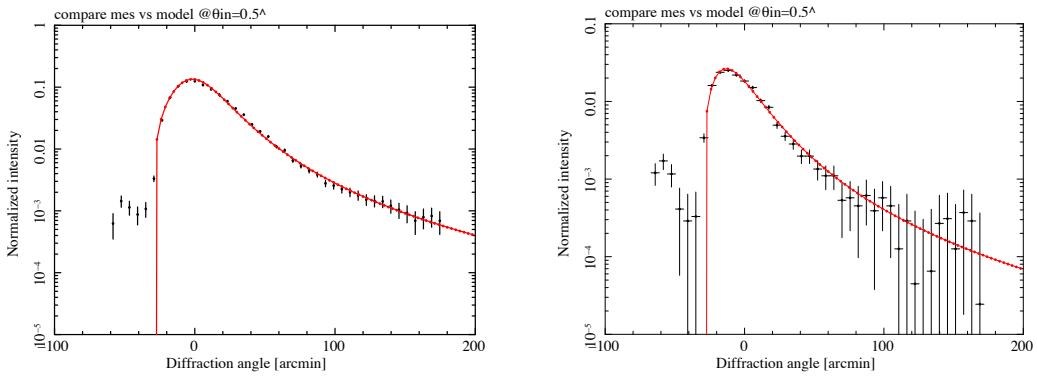

Fig. 2.5 The scattering profile at 1.49 keV of the backside (left) and the pre-collimator (right). The red line corresponds to our model. (Kurashima 2014 Graduation Thesis)

The front-side reflection also shows a variety of the profile shape in small-scale on the arc-minute scale. The profile in small scale varies at each reflector. A pencil beam is illuminated at the local portion of the SXT telescope and some of the resulting images and profiles are shown below in Figure 2.6.
The image is converted into one-dimensional profile along the elongated direction. An example of the profile is shown in Figure 2.7. One notes that the profile is not a single reflection but a double. This double reflection profile is deconvolved into single reflection. The profile is overlaid in Figure 2.7.

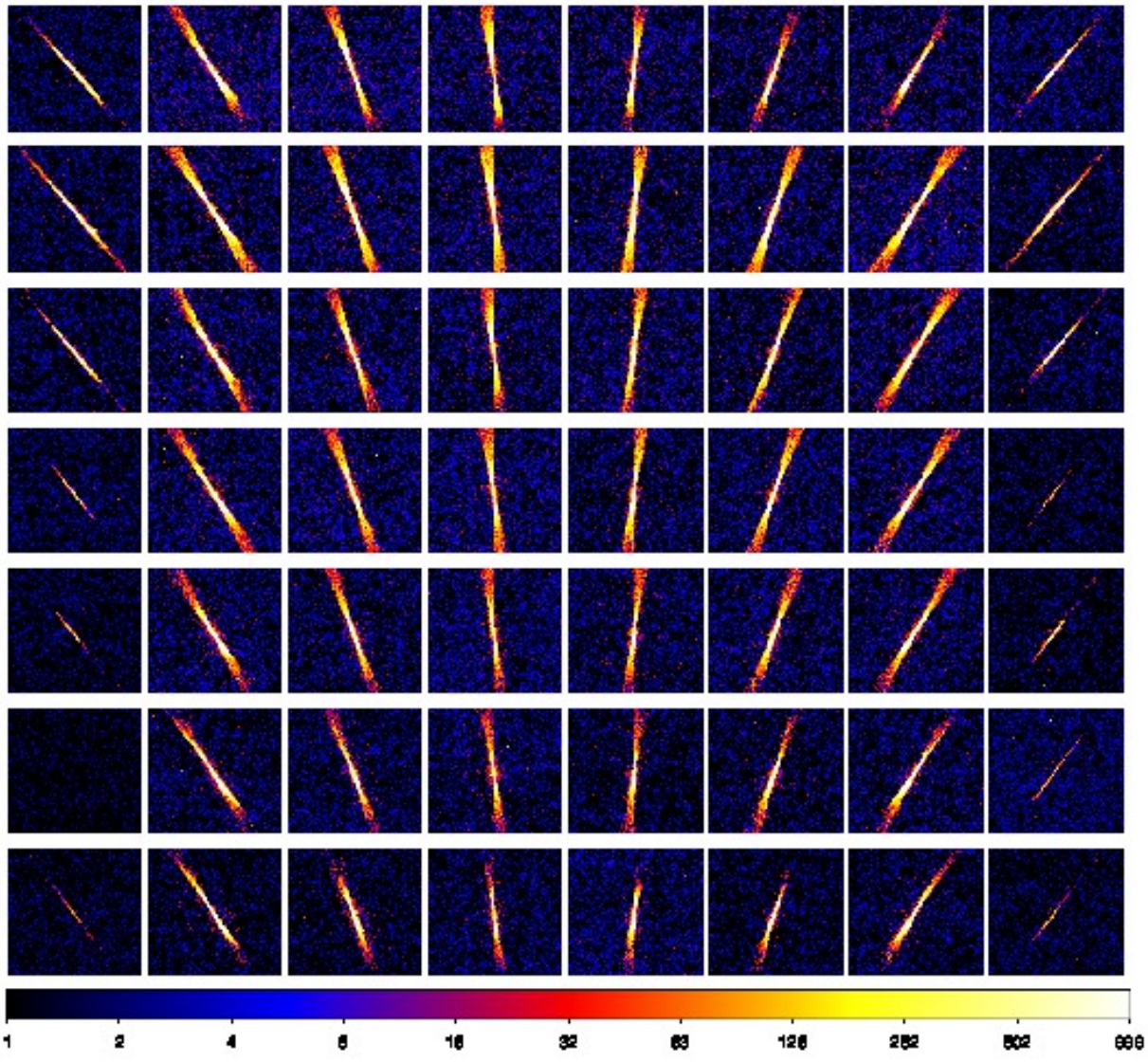

Fig. 2.6 Image of the local portion of the SXT-S's segment 1. The incident energy is 4.5 keV. The image is dominated by double reflections at the front surface. Similar data are obtained from the other segments of SXT-S and SXT-I.

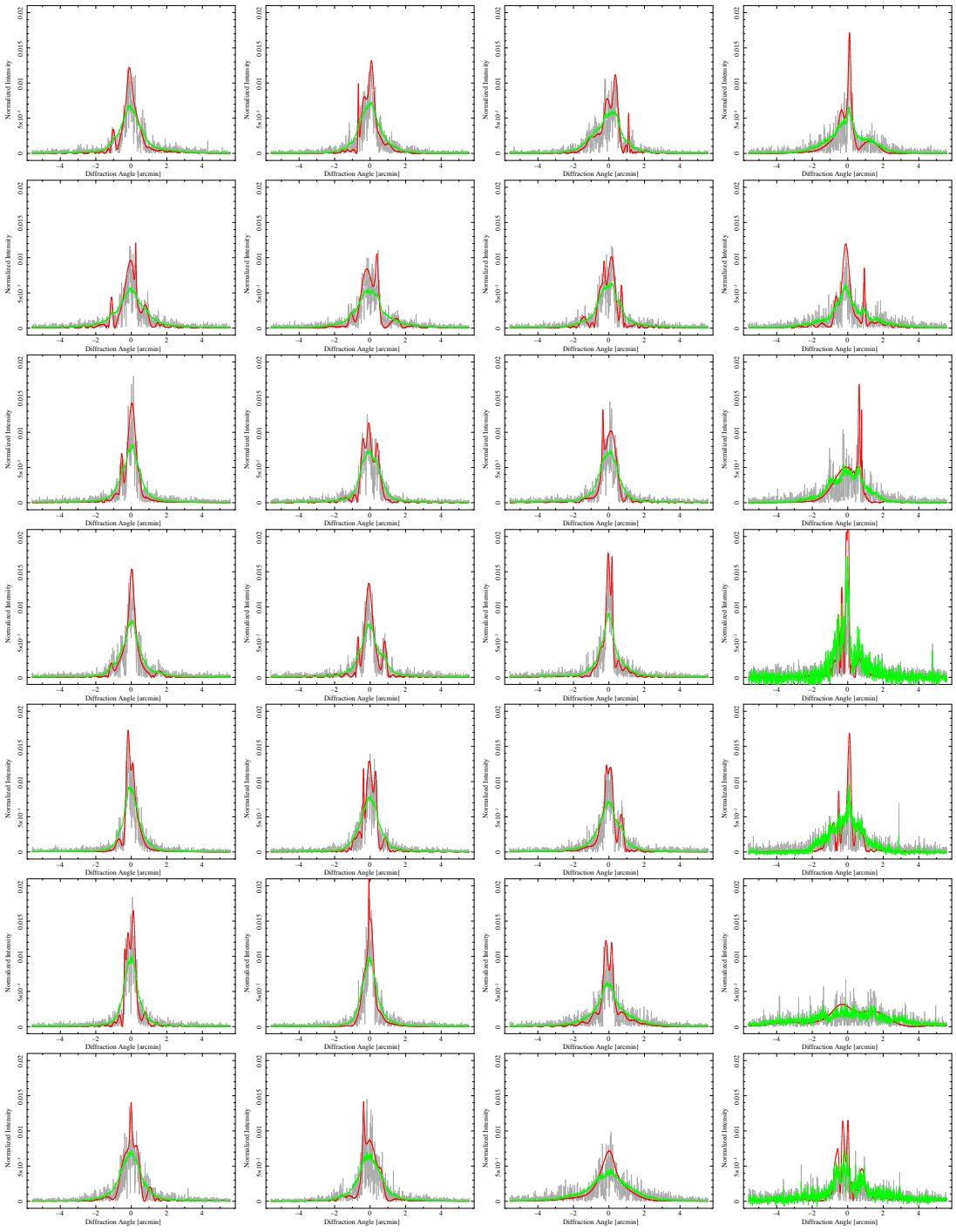

Fig. 2.7 An example of one dimensional profile to the elongated direction of the images above. The green data is the raw profile. The raw data were deconvolved to the single reflection that is plotted with the red color. The black color corresponds to the model.

2.1.3 Over-all performance of the flight module SXT-S/-I

The over-all performance is measured in each segment unit. The measured parameters are (1) optical axis, (2) effective area, (3) vignetting function, and (4) image. The optical axis is defined here as the axis to give a maximum throughput. The position of the optical axis is included as the parameter segment tilt in the tdf file.

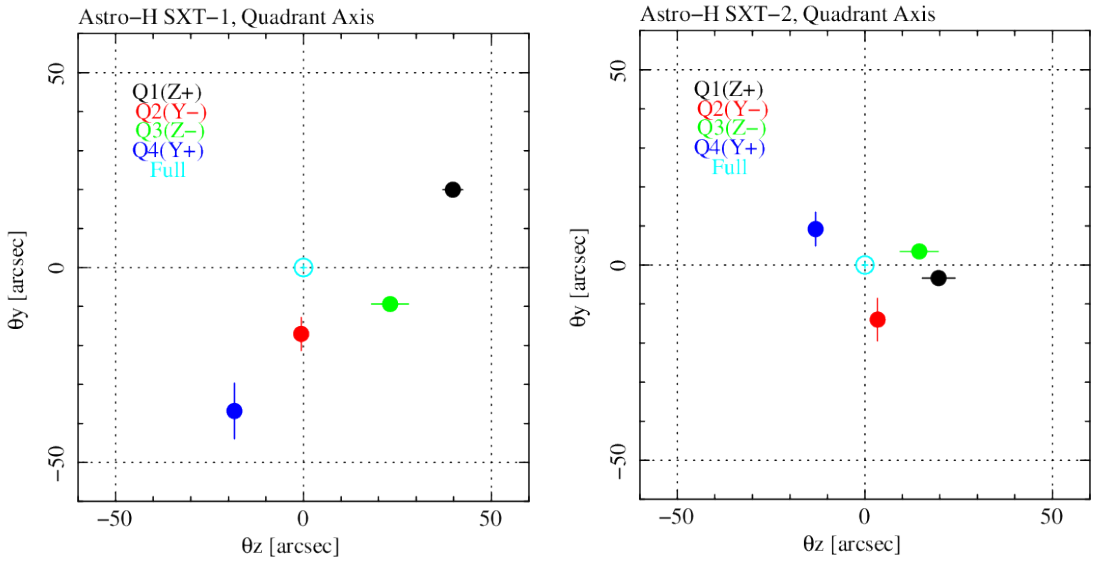

Fig. 2.8 Distribution of the optical axes of the quadrants in the HITOMI SXT-I and SXT-S measure at 4.5 keV. The origin of the coordinate axes is the full-telescope axis. Short and long error bars are corresponding to the directions of the steeper and the flatter angular response, respectively (Iizuka et al. Proc. SPIE 9144, Space Telescopes and Instrumentation 2014: Ultraviolet to Gamma Ray, 914458 (24 July 2014); doi: 10.1117/12.2054626).

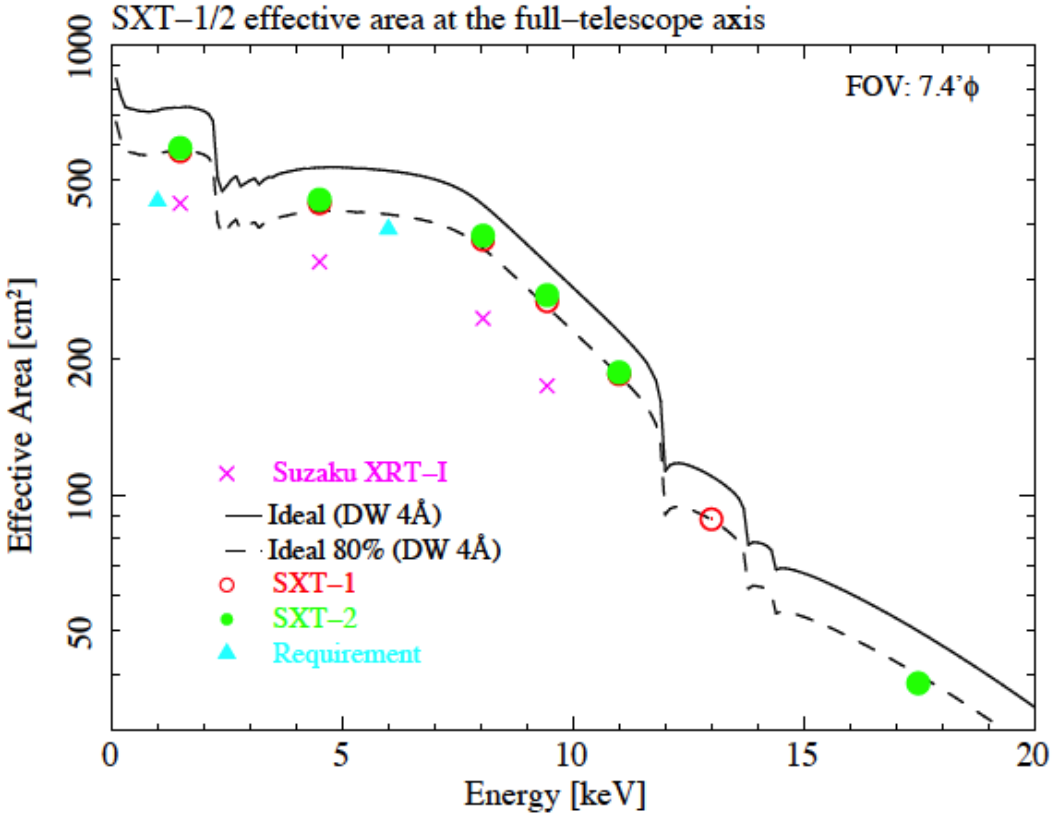

Fig. 2.9 The effective area per telescope of the HITOMI SXT-1(SXT-S) and SXT-2 (SXT-I) at the full-telescope axis. The system requirement of the SXT and the average value of Suzaku SXT-Is are also plotted. The solid and dashed curves show the ideal effective area and the 80% of that calculated from the design parameters, respectively Iizuka et al. Proc. SPIE 9144, Space Telescopes and Instrumentation 2014: Ultraviolet to Gamma Ray, 914458 (24 July 2014); doi: 10.1117/12.2054626.

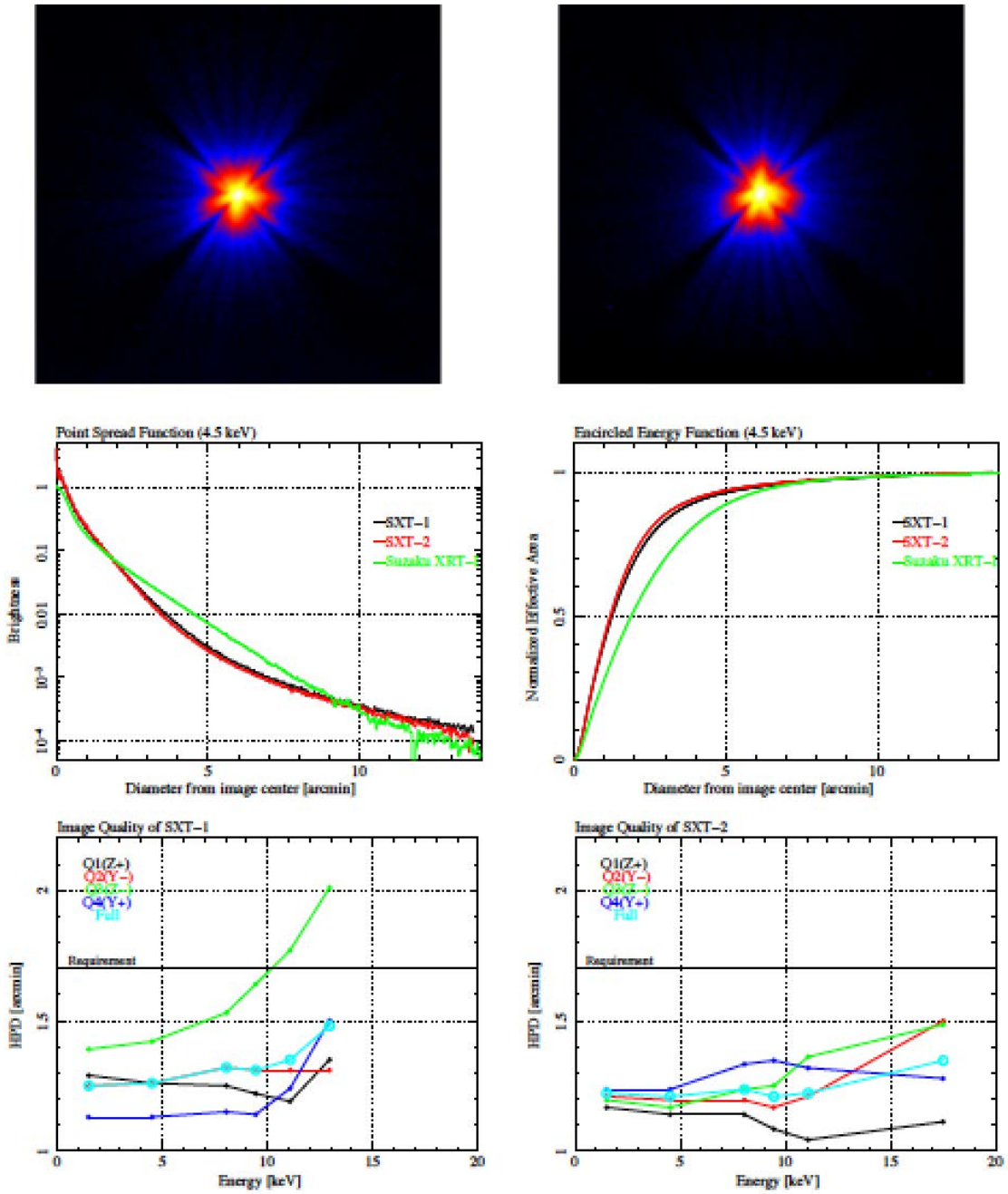

Fig. 2.10 (Top) The X-ray image of at the full-telescope axis of Astro-H SXT-I (left) and SXT-S (right) at 4.5 keV. The image size is 17:1′ x 15’.9. The figures are drawn on a logarithmic scale. (Middle left) Point Spread Function (PSF) of the SXT-I and SXT-S, and Suzaku XRT-I. All the PSFs are normalized by the total ux. (Middle Right) Encircled Energy Function (EEF) of the SXT-I and SXT-S, and Suzaku XRT-I. All the EEFs are normalized to unity at the edge of the detector (CCD). The HPD of the SXT-I and SXT-S is 1.3 and 1.2 arcmin, respectively. That of the Suzaku XRT-Is is ~2 arcmin. (Bottom) Image quality (HPD) of the HITOMI SXT-I (left) and SXT-S (right) at full-telescope axis in unit of arcmin. The statistical errors of HPDs are ~0’.05 (Iizuka et al. Proc. SPIE 9144, Space Telescopes and Instrumentation 2014: Ultraviolet to Gamma Ray, 914458 (24 July 2014); doi: 10.1117/12.2054626).

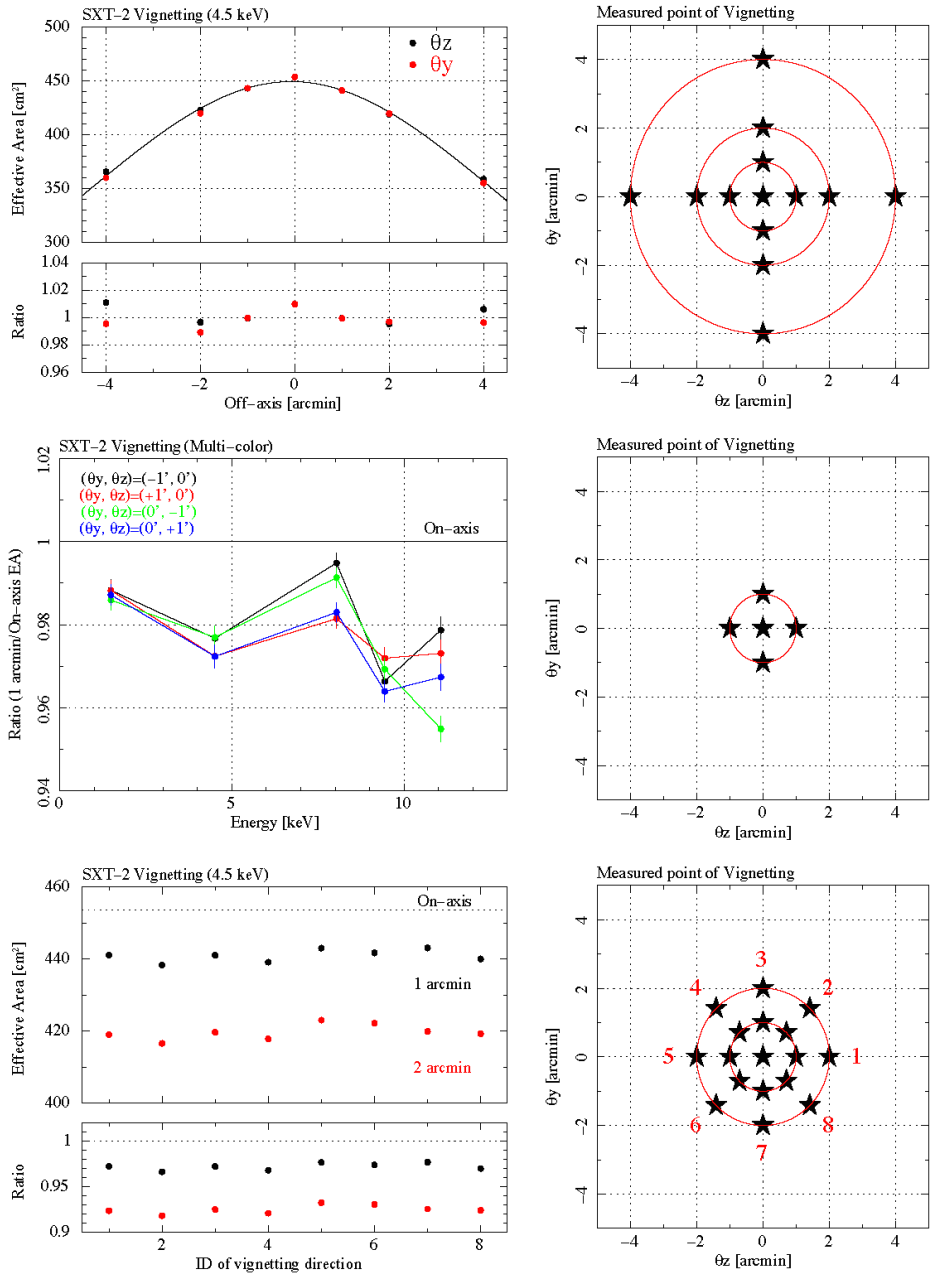

Fig. 2.11 (Top) The off-axis effective area of the SXT-S at 4.5 keV within 4 arcmin off-axis tilting 2 directions at 4.5 keV. The ratio is the measured data fitted with Lorentzian model. The Lorentz width is 16.0 arcmin (FWHM). (Middle) The off-axis effective area at 1 arcmin off-axis tilting 4 points at multi-color. The ratio of the 1 arcmin-off effective area to the on-axis is plotted. The scatter of 4 points is ~1%, but becomes larger as energy's higher. (Bottom) The off-axis effective area at 1 and 2 arcmin off-axis tilting 8 directions. The tilting directions are drawn with ID in right panel. The scatter is ±1% arcmin. (Iizuka et al. 2016).

2.2 Data Analysis

The data are analyzed using ISAS local software.

2.2.1 Optical constants

The optical constant catalog HENKE is first chosen for the optical constant table. However, the energy gap is 30 eV. This value is too big for any SXS data analysis, requiring the need of inserting optical constants around the Gold M and L edges at a finer energy scale. The f1 and

f2 constants as well as the roughness σ, are calculated by fitting the reflectivity curve. The results are given below. Due to the limited capability of KEK data, the f2 constant is interpolated from the HENKE table. The f1 data (labeled 2014KEK) is shown in Figure 2.12.

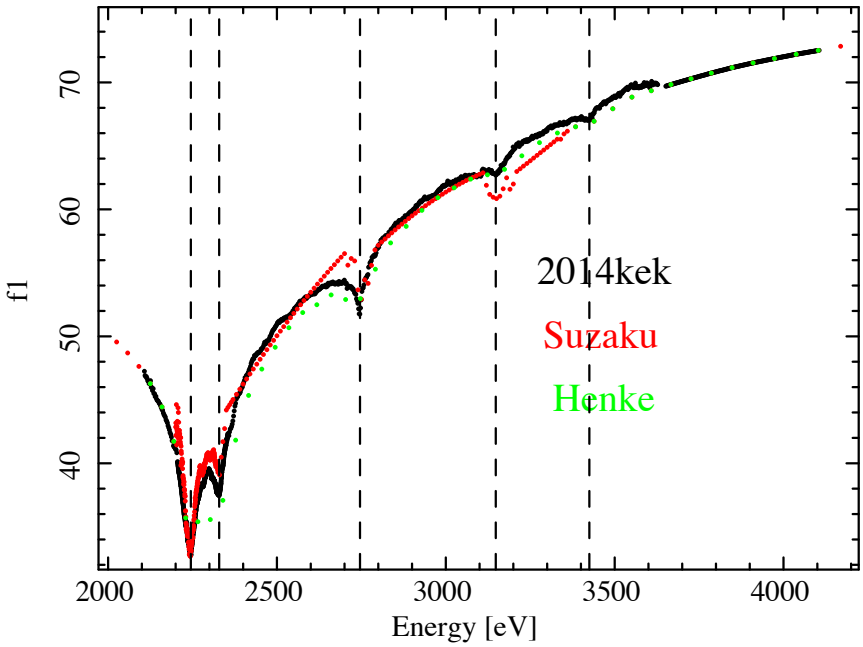

Fig. 2.12 The atomic scattering factor f1 around the gold M-edges. The black data were adapted and is included in the optical constant CALDB file (Kurashima et al. 2016 SPIE, Edinburg).

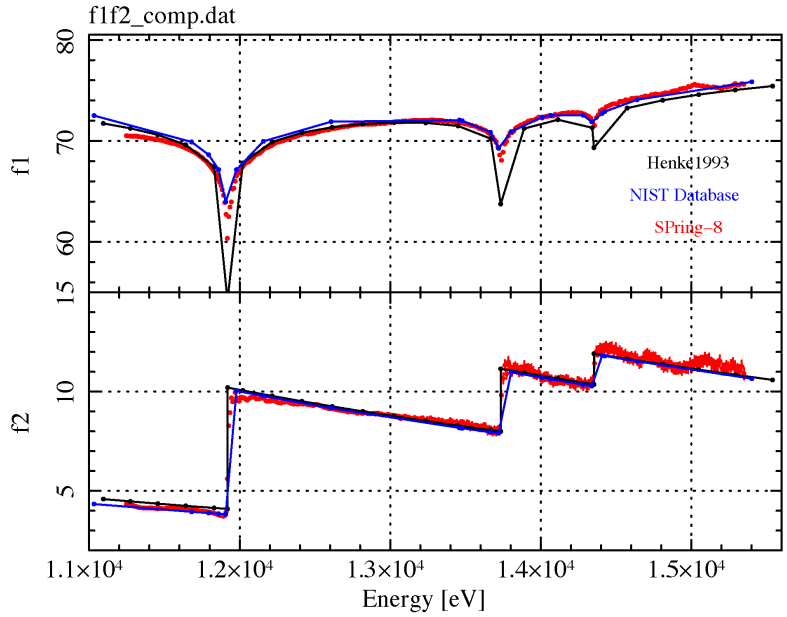

Fig. 2.13 The atomic scattering factor f1 and f2 around the gold M-edges. The red data are adapted and included in the optical constant CADLB file (Kikuchi et al. 2016 in preparation).

2.2.2 Reflectivity

Reflectivity of the front side is calculated using the optical constant in the optical constant table and the roughness in the tdf file. It is recorded as the parameter "RefProb" in the reflectivity tables. In order to cover the long energy band of the SXT, the Gold M and L edge energies are interpolated using HENKE public tables.

The reflectivity of the backside and pre-collimator is empirically modeled by fitting the reflectivity at 1.49 keV. The reflectivity at a given energy is calculated by scaling the incident angle by the wavelength and is recorded in the REFPROBBACK and REFPROBPCOL tables present in the reflectivity file.

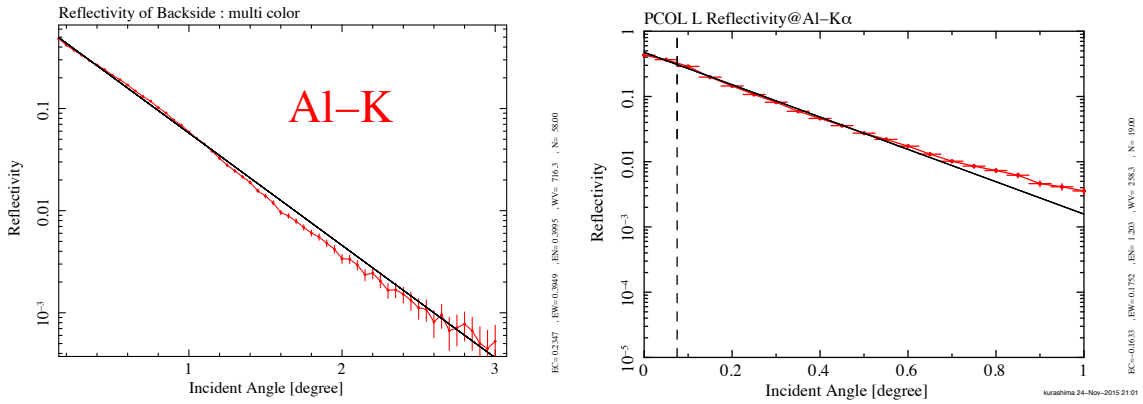

Fig. 2.14 Fitting to the reflectivity measured on ground. Left and right panels show the reflectivity at 1.49 keV of the backside and the pre-collimator, respectively. The black line corresponds to the power-law model we adopted.

2.2.3 Reflection and scattering's profile

By analyzing the reflection profiles in small-scale for the front reflection, we made a map of the image position (right) and image blurring/profile (left) in Fig. 2.16. The image position was modeled by the tilt of the reflector at the position. The tilt number is inserted as the "sector tilt" parameters in the tdf.
The large-scale "scattering profile" in Fig. 2.4 is also modeled. The model of the large-scale scattering profile is merged into that of the small-scale reflection profile. The merged profile is contained in the parameter SCATTER in the scatter file.

For the scattering profiles of the backside and pre-collimator are modeled with the simple models shown in Fig. 2.5. No energy dependence is considered. The scattering profiles are contained the parameter SCATTERBACK and SCATTERPCOL in the scatter file, respectively.

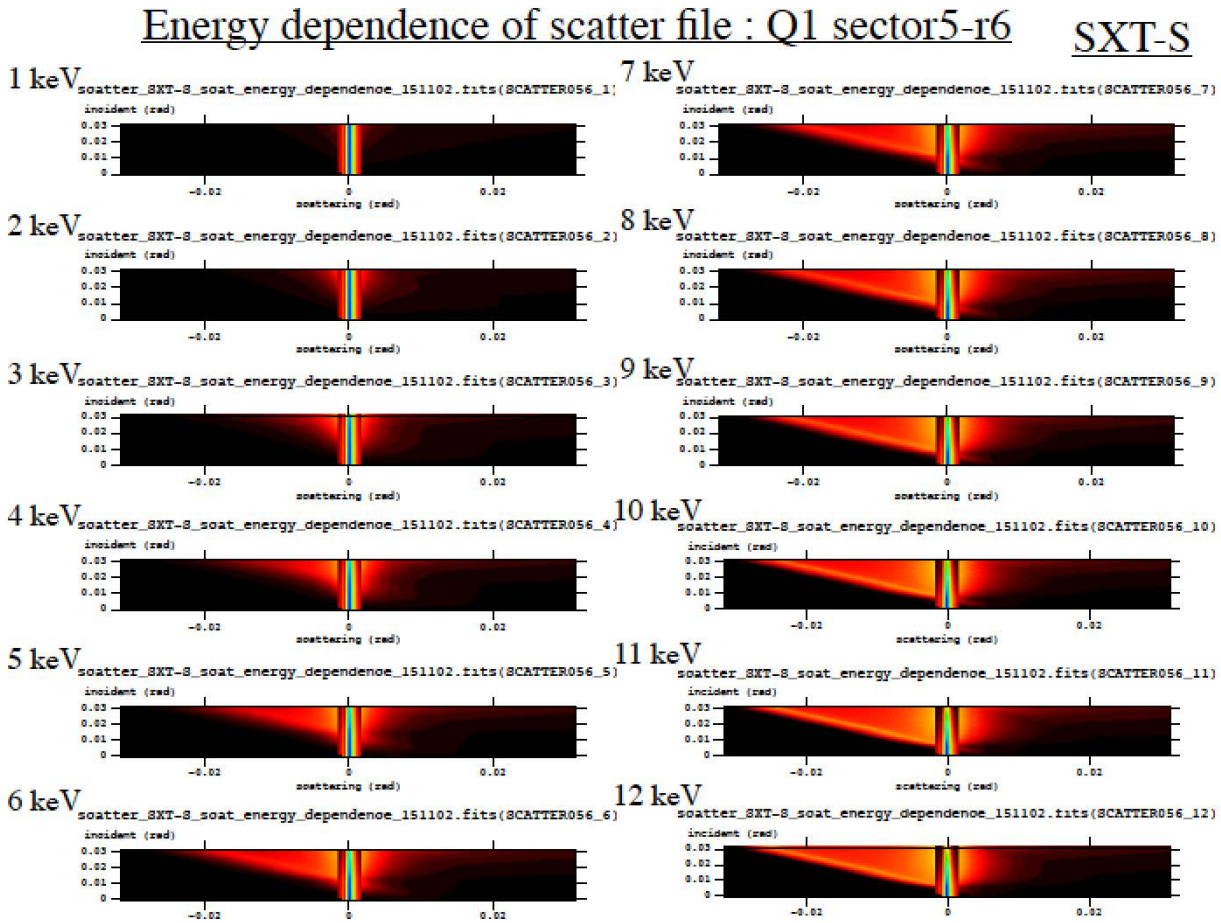

Fig. 2.15 Plots of the scattering profile included as the scatter parameters in the scatter file.

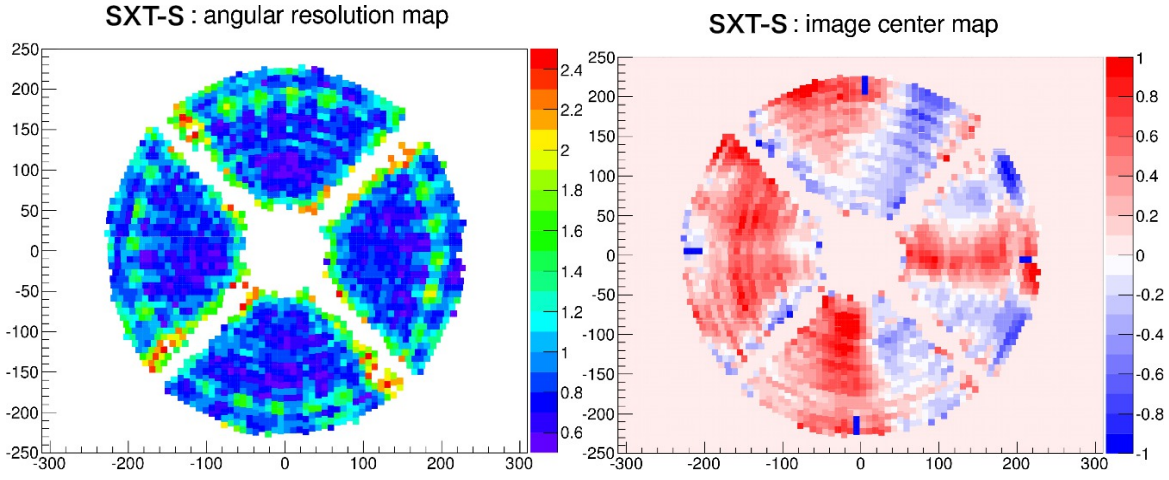

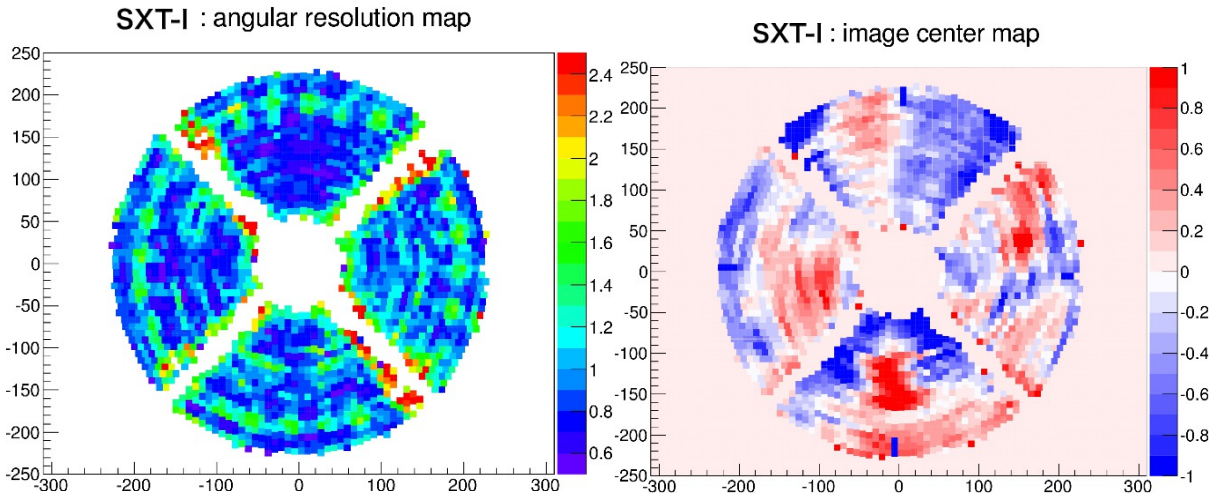

Fig. 2.16 Scattering/reflection tail for the front-side reflection modeled as a function of energy. Upper: SXT-S. Bottom: SXT-I (Sato et al. 2016 submitted to The Applied Optics)

3 Results

Ray-tracing program developed at GSFC/NASA is used to generate the CALDB files for the tdf, scatter and reflection. The effective area, image, and vignetting function are extracted from the ray-tracing output. There are no large difference between the measurements and the ray-tracing simulation software output for the image and the vignetting functions. However, the effective area has a residual of ~10%. This value is minimized by modifying the "segment shift" and "roughness" parameters present in the tdf. The comparison or residual between the measurements and the ray-tracing outputs are listed in the sections below.

3.1 Effective area

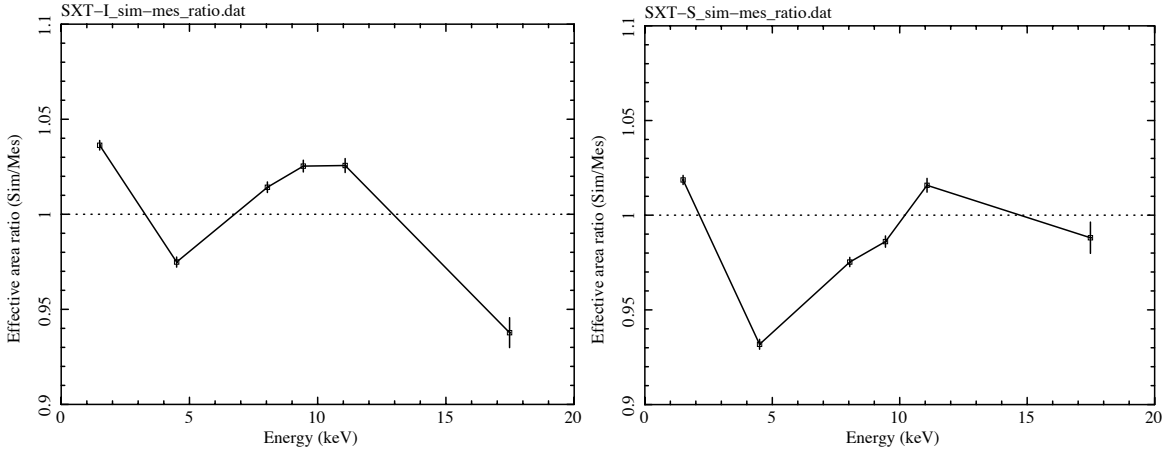

Fig. 3.1 Ratio of the effective area between the measurements and the ray-tracing outputs. Left and right correspond to the SXT-I and SXT-S ratios, respectively.

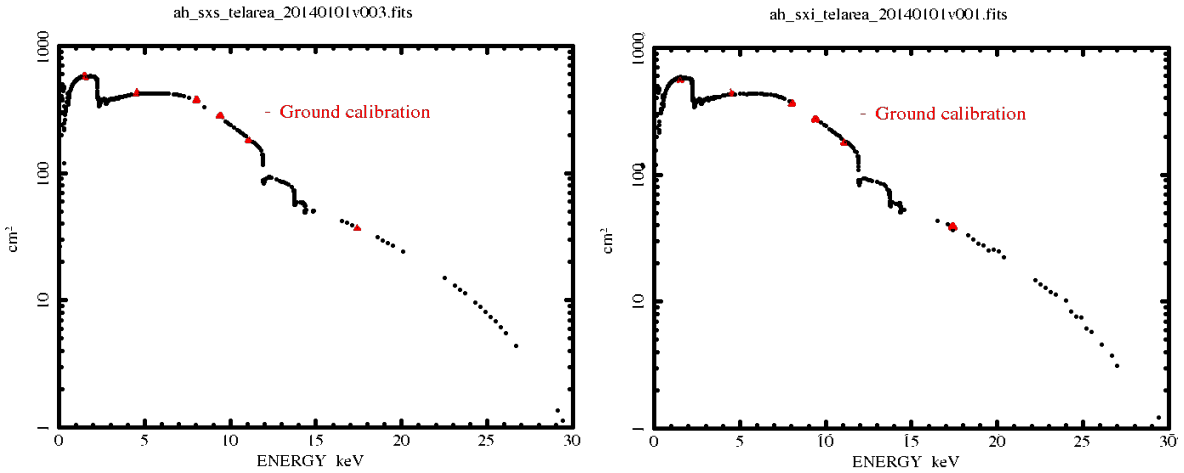

Fig. 3.1b SXS (left) and SXI (right) effective area from the caldb files ah_sxs_telarea_20140101v003 and ah_sxi_telarea_20140101v001 with overlaid the measurements from the ground based-calibration.

3.2 Effective area to the large offset-angle (end-to-end vignetting)

The effective area to the large offset-angle is given below for the SXT-I. The results for the SXT-S are similar to those for the SXT-I. The solid data-points show the data measured on ground whereas the open data-points show the output of the ray-tracing program. In the geometry used for the plots, the detector is located at the on-axis focus position. The integrated area is a circular region and a 12 mm diameter.

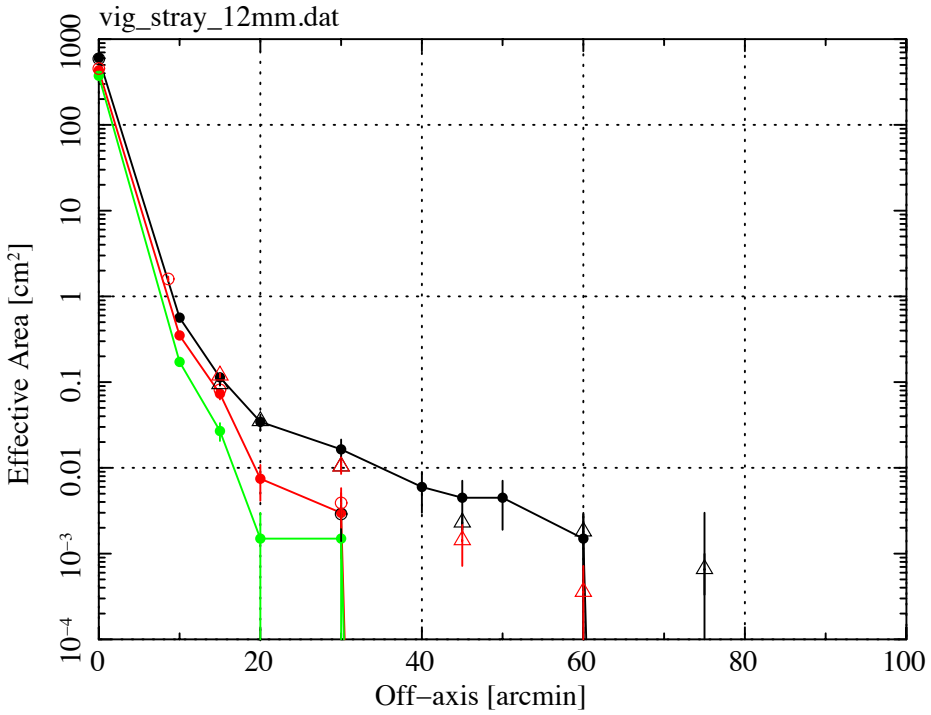

Fig. 3.2 Off-axis effective area in the end-to-end geometry. Black: Al-K, Red: Ti-K, Green: Cu-K. The open circles show data measured on the ground (Iizuka et al. 2016 SPIE, Edinburg). The filled circles correspond to the outputs of the ray-tracing simulator.

3.3 Image on-axis

Comparisons of the PSF between the ray-tracing output and the ground-based calibration at 1.49, 4.51, and 8.04 keV are shown below.

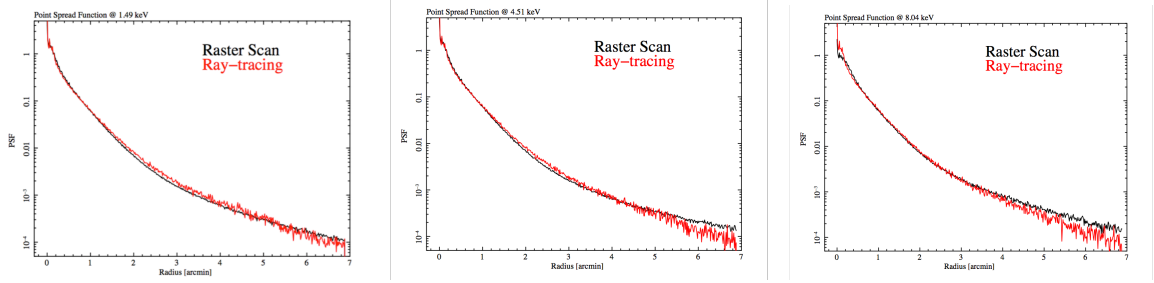

Fig. 3.3 The PSF of the images at 1.49, 4.51, and 8.04 keV. Actual data are plotted in black. Ray tracing outputs in red.

3.4 Analytical modeling

The vignetting curve was tentatively modeled by an analytical function shown in Figure 3.4.

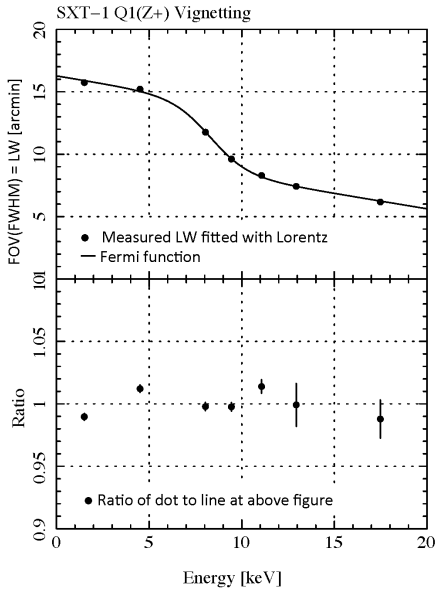

FOV model

- Vignetting(θ,E)
  - Measured data fitted with Lorentz function
    - See next page
  - FOV(FWHM)
    - Lorentz width (LW)

$$f(\theta, E) = 1/(1 + (\frac{2\theta}{LW(E)})^2)$$

- LW(E) model
  - Fermi function
    - Plus Constant + Linear

$$LW(E) = \frac{N}{e^{\beta(E-\mu)} + 1} + C + L * E$$

  - Fitted parameters
    - N=5.77 ['], β=0.98 [1/keV]
    - μ=8.30 [keV]
    - C=10.55 ['], L=-0.25 ['/keV]

Fig. 3.4 The analytical modeling of the vignetting function.

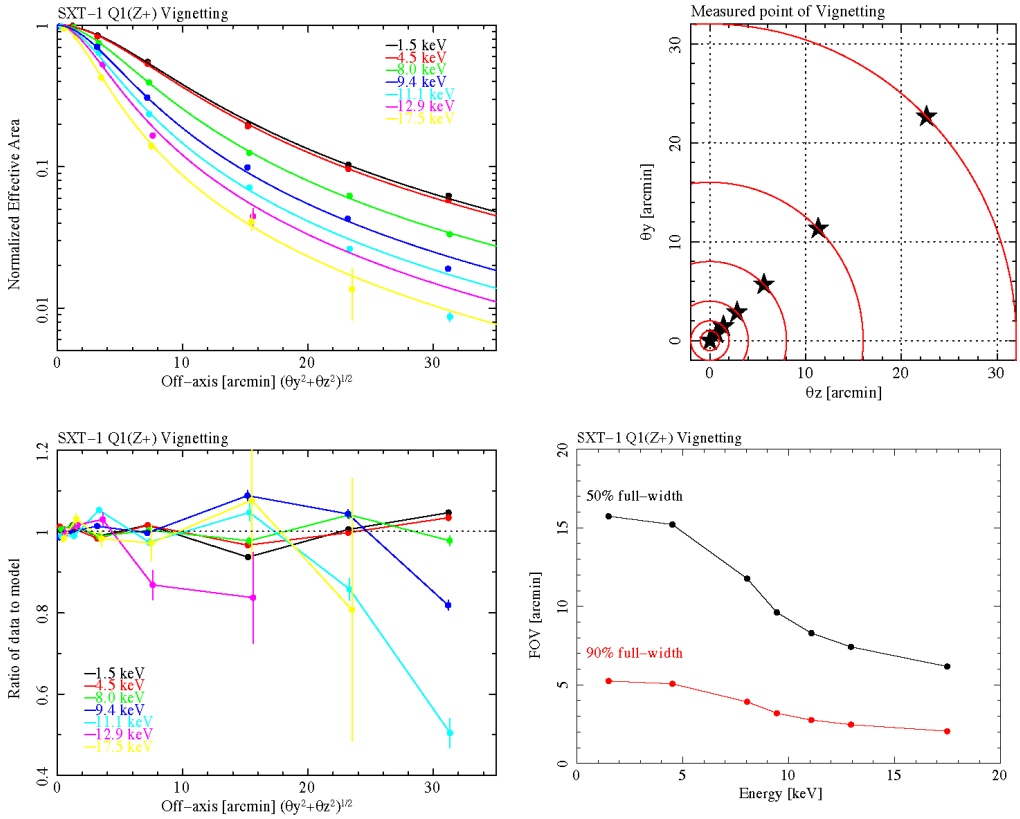

Fig. 3.5 Ratio between model and measurements on ground. Top left: Measurements overlaid with the analytical model. Top right: The direction of the tilt of the segment in the beamline coordinate (see Hayashi et al. 2016 for the definition). Bottom left: The ratio between the model and the measurements. Bottom right: FOV calculated by the model.

3.5 Final remarks

This is the first release of this CALDB file based on ground measurements.